International Journal of Nanomedicine

Dovepress
Taylor & Francis Group

Open Access Full Text Article

ORIGINAL RESEARCH

A Self-Assembling Nanomodulator for Synergistic Therapy of Intracerebral Hemorrhage

Tian Yun[1,2,*], Dan Hou[2,*], Yujie Hu[2], Yonghao Fan[3], Shun Zhang[4], Tiantian Wu[1,4], Yong You[1]

[1]Department of Neurology, The Second Affiliated Hospital of Hainan Medical University, Haikou, People's Republic of China; [2]Department of neurology, Haikou Affiliated Hospital of Central South University Xiangya School of Medicine, Haikou, Hainan, People's Republic of China; [3]Department of General Medicine, West China Lecheng Hospital of Sichuan University, Qionghai, Hainan, People's Republic of China; [4]School of Pharmacy, Hainan Medical University, Haikou, Hainan, People's Republic of China

*These authors contributed equally to this work

Correspondence: Tiantian Wu, School of Pharmacy, Hainan Medical University, Haikou, Hainan, 571199, People's Republic of China, Email sa19071@mail.ustc.edu.cn; Yong You, Department of Neurology, The Second Affiliated Hospital of Hainan Medical University, Haikou, 570311, People's Republic of China, Email hy213440@muhn.edu.cn

Introduction: Intracerebral hemorrhage (ICH) has high mortality and morbidity due to a complex secondary injury phase driven by oxidative stress and excessive inflammation. Given the limited efficacy of singularly-targeted therapies, there is a pressing need for novel therapeutic strategies capable of simultaneously modulating multiple aspects of this pathophysiological network.

Methods: We developed a self-assembled nanomodulator, namely TNF@Gin: Targeted Nano Flower loaded with Ginkgetin (TNF@Gin), by fabricating Ginkgetin-loaded Nano Flowers via Rolling Circle Amplification (RCA). The therapeutic efficacy and mechanisms were systematically evaluated in microglial cells, hippocampal neuronal cells, and an ICH mouse model.

Results: TNF@Gin demonstrated a synergistic regulatory effect by scavenging toxic reactive oxygen species, stimulating the polarization of microglia to the anti-inflammatory M2 phenotype, and inhibiting ferroptosis in hippocampal cells via the Nrf2/GPX4 pathway. In a mouse model of ICH, intravenous administration of TNF@Gin effectively alleviated brain hemorrhage and mitigated ICH-induced behavioral deficits.

Conclusion: The nanomodulator TNF@Gin we developed is a safe and highly effective therapeutic agent for ICH synergistic therapy. To the best of our knowledge, this study represents the first RCA-based drug delivery system for ICH synergistic treatment, offering a novel and promising therapeutic strategy that synergistically targets inflammation and ferroptosis.

Keywords: nanomedicine, DNA nanotechnology, biomaterials, ICH synergistic therapy

Introduction

Intracerebral hemorrhage (ICH), as the spontaneous, non-traumatic rupture of a blood vessel within the brain parenchyma, is a devastating neurological condition accounting for approximately 10–15% of all strokes.[1–3] Despite advances in medical management, ICH continues to be associated with the highest mortality and morbidity rates among all stroke subtypes, leaving a majority of survivors with long-term neurological disabilities. The pathophysiological cascade of ICH is biphasic, encompassing an initial primary injury followed by a more prolonged and complex secondary injury phase. Following the initial hemorrhage, the breakdown of red blood cells leads to the substantial release of hemoglobin and its degradation products, liberating a massive amount of iron into the extracellular space.[2,4–6] This iron overload is a potent catalyst for oxidative stress through the Fenton reaction, generating highly reactive hydroxyl radicals that induce lipid peroxidation and trigger ferroptosis, a newly defined and iron-dependent form of regulated cell death.[7–9] Ferroptosis has been implicated in the death of neurons, oligodendrocytes, and endothelial cells, contributing significantly to blood-brain barrier (BBB) disruption, cerebral edema, and long-term neurological deficits.[10–12] The secondary injury phase, evolving over hours to days following the initial bleed, is now recognized as the primary determinant of clinical outcome and a key target for therapeutic intervention. This phase is driven by a complex interplay of pathological processes, including

https://doi.org/10.2147/IJN.S590652
Received: 9 January 2026
Accepted: 13 March 2026
Published: 16 March 2026

inflammation, oxidative stress, and programmed cell death. Concurrently, the hematoma and its degradation products act as potent danger-associated molecular patterns, initiating a robust and sustained inflammatory response.[3,13,14] Central to this response is the rapid activation and infiltration of immune cells, particularly microglia and peripherally derived macrophages. These cells exhibit profound phenotypic plasticity, polarizing into distinct functional states. The classically activated M1 phenotype releases pro-inflammatory cytokines (eg., TNF-α, IL-1β), exacerbating neuroinflammation and secondary injury.[2,3,14] In contrast, the alternatively activated M2 phenotype secretes anti-inflammatory cytokines (eg., IL-10, TGF-β), promoting tissue repair, debris clearance, and angiogenesis.[15,16] The balance between these macrophage phenotypes is a critical determinant of ICH prognosis; a persistent M1-dominant state is associated with poor outcomes, while a timely transition to an M2 phenotype is neuroprotective.[17–19] The convergence of ferroptosis and excessive inflammation creates a vicious cycle that amplifies secondary brain damage. Given the limited efficacy of singularly-targeted therapies,[11,12,18,19] there is a pressing and unmet need for novel therapeutic strategies capable of simultaneously modulating multiple aspects of this complex pathophysiological network. Interventions designed to attenuate inflammation, scavenge iron, protect the BBB, and inhibit cell death pathways hold immense promise for improving functional recovery and reducing the global burden of this devastating disease.

The advent of nanomedicine has revolutionized therapeutic strategies by enabling the precise delivery of bioactive agents to disease sites, thereby enhancing efficacy while minimizing systemic toxicity.[20,21] Traditional nanodelivery systems, such as liposomes and polymeric nanoparticles, have made significant strides in improving the pharmacokinetic profiles of encapsulated drugs. However, the growing complexity of modern therapeutics, which often require the synergistic action of multiple components as targeting ligand, therapeutic payload, and functional modulator, has exposed the limitations of conventional delivery platforms.[21–23] These systems frequently suffer from low loading capacity, uncontrolled stoichiometry, and cumbersome, multi-step conjugation chemistries that can compromise batch-to-batch consistency and biological activity. To overcome these challenges, the field has shifted towards the development of next-generation, programmable nanomaterials that can integrate multiple functional components in a defined and efficient manner. Among these, nanostructures constructed through Rolling Circle Amplification (RCA) have emerged as a particularly promising platform. RCA is an isothermal, enzymatic method for producing long, single-stranded DNA composed of tandem repeats, which can then self-assemble into highly ordered, flower-like nanostructures.[22,24,25] The inherent properties of this biosynthetic process confer unparalleled advantages for multi-component integration. Firstly, the RCA template itself can be rationally designed to incorporate functional nucleic acid sequences, such as aptamers for targeted delivery, siRNA or antisense oligonucleotides for gene silencing, or DNAzyme for catalytic therapy.[26–28] This allows the DNA or RNA-based therapeutic or targeting function to be encoded directly into the scaffold's backbone, ensuring precise stoichiometric control. Secondly, the dense, highly porous, three-dimensional architecture of the nano-flower provides an exceptionally high surface area and an abundance of interstitial binding sites. This enables the efficient physical adsorption or intercalation of a wide range of therapeutic cargos, including small-molecule drugs, proteins, and photosensitizers, leading to markedly higher loading capacities compared to conventional carriers. Consequently, RCA Nano-flowers represent a paradigm shift from simply "carrying" drugs to "integrating" complex therapeutic regimens, offering a powerful and versatile tool for developing sophisticated, multi-modal treatments for complex diseases like cancer, neurodegenerative disorders, and infections.[29,30] To the best of our knowledge, there have been no reports on the use of RCA nano-flowers for the treatment of ICH, suggesting that this multifunctional nano-flower-based delivery system holds great potential.

Standardized extracts from *Ginkgo biloba* have been extensively used for their neuroprotective and cardioprotective benefits. Ginkgetin was chosen for this investigation owing to its potent reactive oxygen species (ROS)-scavenging activity, which plays a pivotal role in alleviating oxidative stress associated with chronic diseases.[31] Herein, we developed a self-assembled nanomodulator TNF@Gin (Targeted Nano Flower loaded with Ginkgetin) for the treatment of ICH by targeted delivery of Ginkgetin (Figure 1). Based on RCA technology, we fabricated Nano Flowers containing a hybridization site for modifying DNA nanostructure (T structure) containing 3 copies of transferrin receptor-targeted aptamer, endowing the delivery system with the capability to cross the BBB and accumulate at the site of injury. The Ginkgetin were loaded through non-covalent interactions, enabling high loading efficiency under mild and simple operational conditions. This nanomodulator was found to exert a synergistic regulatory effect, combining hippocampal

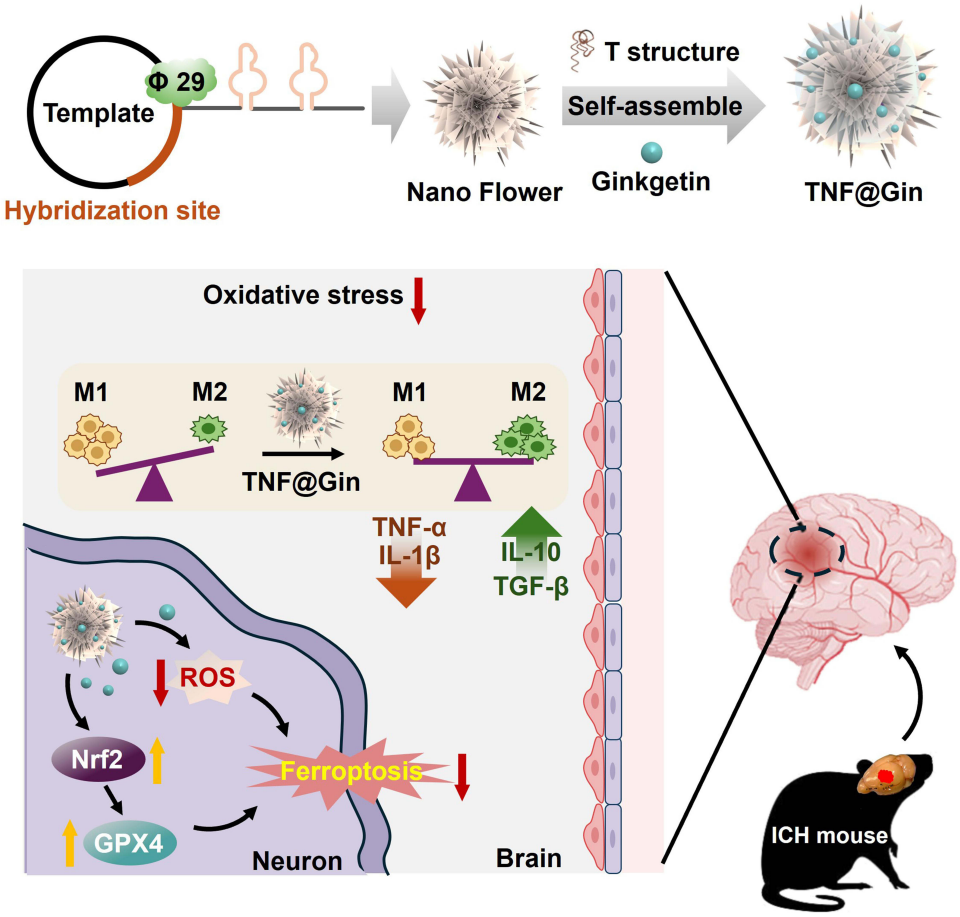

Figure 1 Schematic presentation of the Ginkgetin-loaded self-assembly nanoplatform TNF@Gin for intracerebral hemorrhage (ICH) treatment. Red downward arrows indicate downregulation, while yellow upward arrows indicate upregulation.

Abbreviations: TNF@Gin, Targeted Nano Flower loaded with Ginkgetin; φ29, phi29 DNA polymerase as cornerstone enzyme for isothermal nucleic acid amplification techniques in rolling circle amplification; TNF-α, tumor necrosis factor-α; IL-1β, interleukin-1β; IL-10, interleukin-10; TGF-β, transforming growth factor-β; ROS, reactive oxygen species; GPX4, glutathione peroxidase 4; Nrf2, nuclear factor erythroid 2-related factor 2.

cells protection with microglial cells polarization. By efficiently inhibiting oxidative stress, the treatment of TNF@Gin promotes the polarization of microglia to the anti-inflammatory M2 phenotype, thereby reducing the levels of pro-inflammatory factors. Concurrently, TNF@Gin inhibits hippocampal cell ferroptosis through combining potent ROS scavenging with the modulation of the Nrf2/GPX4 signaling pathway. In a mouse model of ICH, intravenous administration of the nanomodulator effectively alleviated brain hemorrhage. Through the synergistic regulation, TNF@Gin mitigated the behavioral deficits induced by ICH, demonstrating a highly effective and safe therapeutic outcome. The development of the multifunctional nanomodulator offers a novel strategy for the construction of ICH therapeutic agents.

Materials and Methods

Materials

All mentioned oligonucleotides and triphenylphosphine-modified DNA were purchased from Hu zhou Hippo Biotechnology Co., Ltd. DCFH-DA and dithiothreitol (DTT) were purchased from Aladdin (Shanghai). Ginkgetin (566.52 Da, purity >98%) and oxyhemoglobin (OxyHb) was purchased from Merck & Co, Inc. DMEM/F12, trypsin, and fetal bovine serum (FBS) were purchased from Gibco™. Antibodies and fluorescent probe-labeled secondary antibody were purchased from (Abcam; Cambridge, MA). Cell culture dishes/plates, round coverslips, and 20-mm glass-bottom dishes were obtained from NEST Biotechnology Co. Ltd. (Wuxi, China). YeaRed Nucleic Acid Gel Stain (cat#10202ES76), phi29 DNA polymerase (cat#14404ES72), and Hifair® One Step RT-qPCR SYBR Green Kit

https://doi.org/10.2147/IJN.S590652

(cat#11143ES70) were purchased from Yeasen, Shanghai, China. Hochst33258 (C0020) and cell counting kit 8 (CCK-8) were purchased from Beijing Solarbio Science & Technology Co.,Ltd. ABclonal ELISA Kit (RK08016, RK09250, RK09263, and RK09283) were purchased from ABclonal Technology (WuHan, China).

Cells

All cell lines mentioned were purchased from the American Type Culture Collection (ATCC). To establish the in vitro ICH model, HT22 and BV2 cells with OxyHb were stimulated with 20 μM OxyHb and 5% CO_2 at 37 °C following the reported procedures.[17]

Design of the DNA Template and T Structure

The linear DNA template containing the hybridization site (GTGCTACTCCAGTTC) was synthesized by solid-phase synthesis with phosphate at the 5′ site (Figure S1A). To construct the T structure, the DNA self-assembly Y shape was designed with 3 extended DNA strands containing the aptamer sequence (GAATTCCGCGTGTGCACACGGTCACAGTTAGTATCGCTACGTTCTTTGGTAGTCCGTTCGGGAT) as shown in Figure S1B, and the detailed DNA sequence was included in the supporting Table S1.

Preparation of the DNA Nanomodulator TNF@Gin

The preparation of the nano flower was based on the RCA reaction as described.[28,29] Typically, 2 μM 5′ phosphorylated DNA templates and equivalent primer were mixed and annealed in 1 × T4 DNA ligation buffer (50 mM Tris-HCl, 10 mM $MgCl_2$, 10 mM DTT, and 1 mM adenosine triphosphate (ATP), pH = 7.5), followed by the addition of T4 DNA ligase (10 U/μL) and incubation at 16 °C for 12 h. Subsequently, the ligated circular DNA templates (0.3 μM) were incubated with dNTPs (1 mM) and phi29 DNA polymerases (1 U/μL) in the corresponding reaction buffer (50 mM Tris-HCl, 10 mM $MgCl_2$, 66 mM KCl, 0.04% (v/v) Tween 20, 4 mM DTT, pH = 7.5) at 30 °C for 18 h.

To synthesize the T structure, the purified DNA strands (L, S1-1, S1-2, S1-3, S1, S2, S3, 1–4, 1–5, and 1–6) were mixed at the same molar ratio in a 1×TAE/Mg^{2+} buffer (40 mM Tris, 20 mM acetic acid, 2 mM EDTA, and 12.5 mM magnesium acetate, pH = 8.3) with a concentration of 1 μM. The aforementioned assembly solutions were kept at 95 °C for 3–5 min and then cooled down from 95 to 25 °C over 24 h. Then, 10 nM of T structure was mixed with Nano Flower at 25 °C for 9 h for hybridization.

After hybridization, the drug loading procedure for preparing TNF@Gin was conducted by directly adding the component Ginkgetin. To optimize the loading of the therapeutic drug, Ginkgetin ranging from 0.1 to 1.5 mg/mL was added with different culture times (1.0 to 6.0 h). After the incubation, the mixture was washed with PBS by centrifugation at 8500 rpm for 5 min and stored at 4 °C. The drug loading efficiency (DLE) was measured by UV absorption and calculated (DLE %=(Ginkgetin added-free Ginkgetin)/(Ginkgetin added)×100%).

Prepared TNF@Gin (1μg/mL in ddH_2O) was deposited onto a copper grid. After deposition for 0.5 h, the excess sample solution was then removed. The grid was dried overnight and sputter-coated with gold before observation. The images were collected and processed using a Hitachi SU8220 Scanning Electron Microscope. For Atomic force microscopy (AFM) imaging, the freshly prepared TNF@Gin (1μg/mL) was deposited onto mica and deposited for 3 min. After deposition, the surface of the mica was rinsed with 1 mL ddH_2O and air-dried. The prepared samples were imaged with a MultiMode 8 AFM (Bruker) under ScanAsyst-Air mode. Dynamic light scattering (DLS) analysis of Nano flower and TNF@Gin was performed on a Malvern Zetasizer Nano-ZS (Malvern Instruments, U.K.) at 25 °C.

Stability Analysis

TNF@Gin (10 μg/mL) was incubated in DMEM with 10% FBS for 0 to 24 h at 37 °C. Then, the samples were characterized by DLS to measure the particle size and distribution at 25 °C and 0.8% agarose gel electrophoresis to verify the aggregation and degradation.

Drug Release Analysis

Freshly prepared TNF@Gin was re-suspended in 1 mL of PBS and sealed within a pre-soaked dialysis bag (MWCO: 5 kDa). The dialysis bag was then fully immersed in 5 mL of PBS with different pH value and further incubated at 37 °C under constant gentle agitation. The concentration of the released drug in the collected samples was quantified using UV-Vis spectrophotometry (λ=352 nm, without interfering with the absorption peak of DNA at 260 nm).

Cell Viability Assay

ICH cells (HT22 cells or BV2 cells stimulated with OxyHb) incubated with different drugs were tested using the CCK 8 kit. The OD value was measured at the wavelength of 450 nm.

Determination of Intracellular ROS

In this study, intracellular ROS generation was measured using a DCFH-DA assay. Cells were seeded in confocal plates (1×10^5 cells) and, after adhesion, treated with various drugs for 12 h. Following treatment, cells were incubated with DCFH-DA according to the manufacturer's instructions, washed three times with cold PBS, and imaged using a fluorescence microscope (Ex/Em = 488/525 nm).

ELISA Assay

Levels of the inflammatory factors Tumor Necrosis Factor-α (TNF-α), Interleukin-1β (IL-1β), Interleukin-10 (IL-10), and Transforming Growth Factor-β (TGF-β) were quantified using an Enzyme-Linked Immunosorbent Assay (ELISA). To prevent protein degradation, supernatants from the culture medium and peri-hematomal brain tissues were collected and stored at −80 °C. All measurements were performed with an ELISA Array Kit in strict accordance with the manufacturer's instructions.

Animal Experiment Ethics

C57 mice (6–8 weeks old) were purchased from Vital River Laboratory Animal Technology Co., Ltd. All animals received care in compliance with the guidelines outlined in the Guide for the Care and Use of Laboratory Animals. The procedures were approved by the Institutional Animal Care and Use Committee of Hainan Medical University with ethics approval (HYLL-2024-253). Mice were anesthetized with isoflurane (4–5% for induction, 1.5–2% for maintenance) in oxygen (1 L/min) using standard inhalation equipment. Euthanasia was performed by CO_2 inhalation using a gradual displacement method (20–30% chamber volume per minute) until 100% CO_2 concentration was achieved. All anesthesia was performed following AVMA guidelines.

In vivo Therapeutic Effect Assay

The ICH mouse model was induced in 6-week-old C57BL/6 mice via stereotactic injection of 0.08 units of collagenase VII (0.08 U in 1.0 μL saline) into the striatum as reported.[17,32] Seven days post-injury, mice were randomly assigned to four groups (PBS, Nano Flower, Ginkgetin, and TNF@Gin) and administered intravenous injections of the respective formulations (50 μL) on days 0, 2, and 4. The dosage was calculated as 2 mg Ginkgetin/kg body weight. Body weight and behavioral deficits were monitored throughout the treatment. Upon completion of the regimen, mice were euthanized for brain tissue collection and subsequent analysis.

Staining of Tissue Sections

Mouse organs were fixed in 4% paraformaldehyde at room temperature, paraffin-embedded, and sectioned at 5 μm. The sections were then stained with Hematoxylin and Eosin (H&E) for morphological examination. For immunofluorescence, harvested brain tissues were similarly sectioned at 5 μm and mounted onto slides. Immunostaining was performed according to the manufacturer's standard protocol.

Statistical Analysis

All data are expressed as mean ± s.d., and for comparisons between two groups, means were compared using the one-way analysis of variance (ANOVA) with the Tukey post hoc test.

Results and Discussion

Preparation and Characterization of the Nanomodulator TNF@Gin

For neuroprotective and cardioprotective properties, standardized extracts derived from the leaves of *Ginkgo biloba* have been extensively used in both traditional and modern medicine. The therapeutic potential of the biflavone components (Ginkgetin, Isoginkgetin, and Bilobetin) stems from their multifaceted mechanisms of action. They are widely recognized for their potent antioxidant properties, effectively scavenging ROS and upregulating endogenous antioxidant defense systems like the Nrf2 pathway as reported.[31] This activity is crucial in mitigating oxidative stress, a key pathological driver in numerous chronic diseases. Furthermore, Ginkgetin exhibits significant anti-inflammatory effects by modulating key signaling pathways, thereby reducing the production of pro-inflammatory cytokines.[33] Therefore, in this study, we utilized Ginkgetin to fabricate a nanomodulator aimed at addressing the therapeutic challenges of ICH as shown in Figure 1. To achieve blood-brain barrier penetration, we designed a template containing a hybridization site for modification of the T-structure, which incorporates a TfR-targeted aptamer for BBB crossing (Figure S1). This template was then subjected to RCA to form a nanoscale assembly (Nano Flower), which was subsequently modified with the T-structure and loaded with Ginkgetin. Multiple copies of aptamers on the T-structure enable surface modification of the nano-platform with targeting ligands and facilitate ligand-receptor binding. To characterize the drug-loading capabilities of the nanomodulator TNF@Gin, comprehensive analyses were conducted. First, to determine the optimal drug-loading capacity, we investigated the effect of varying the initial concentration of Ginkgetin during the synthesis process. As shown in Figure 2A, the loading amount of Ginkgetin increased proportionally with the initial feeding concentration up to 1.0 mg/mL. Furthermore, prolonged incubation time was beneficial for drug loading. Based on this, the optimal DLE was determined to be 47.83% using UV absorption spectroscopy (Figure 2B). Similar to our previous study, Ginkgetin, as a biflavone, is loaded onto Nano Flowers via non-covalent binding, primarily through intercalation.[34,35] The morphology and topography of the synthesized TNF@Gin were then visualized using electron and atomic force microscopy. SEM (Scanning electron microscopy) revealed that the TNF@Gin possessed a well-defined, uniform flower-like nanostructure (Figure 2C). Atomic force microscopy (AFM) and Transmission electron microscope (TEM) further confirmed the monodispersity, corroborating the SEM observations (Figures 2D, S2–S4). Next, the hydrodynamic properties and surface charge of the nanoplatform were evaluated in a physiological environment. DLS analysis in PBS showed that the TNF@Gin exhibited a narrow hydrodynamic size distribution with an average diameter of approximately 135.8 ± 14.6 nm, which is favorable for potential in vivo applications (Figure 2E). Furthermore, zeta-potential measurements exhibited a zeta-potential shift following the successful loading of Ginkgetin, confirming the successful drug-loading (Figure 2F). Finally, the drug release profile of TNF@Gin was measured under different pH conditions to simulate various physiological environments. As shown in Figure 2G, the nanomodulator exhibited a time-dependent sustained-release behavior, indicating that the therapeutic agents can be released continuously to maintain an effective drug concentration, thereby ensuring sustained pharmacological activity. Moreover, the TNF@Gin maintained its particle size and dispersibility under both static and shaking conditions, indicating the excellent stability under a physiological environment (Figures S5 and S6).

M1/M2 Microglial Polarization Effect of the Nanomodulator

To evaluate the therapeutic potential of TNF@Gin in mitigating oxidative stress and modulating microglial polarization, we established an in vitro ICH model using BV2 cells stimulated with OxyHb. After confirming the effective cellular internalization, we assessed the intracellular ROS levels regulated by TNF@Gin in ICH cells (Figures S7 and S8). As visualized by DCFH-DA fluorescence, cells induced by OxyHb exhibited a significant increase in ROS production compared to the untreated control (Figures 3A and S9). While the Nano Flower and free Ginkgetin offered moderate reduction in ROS levels, the TNF@Gin group demonstrated the most potent antioxidant effect, with fluorescence

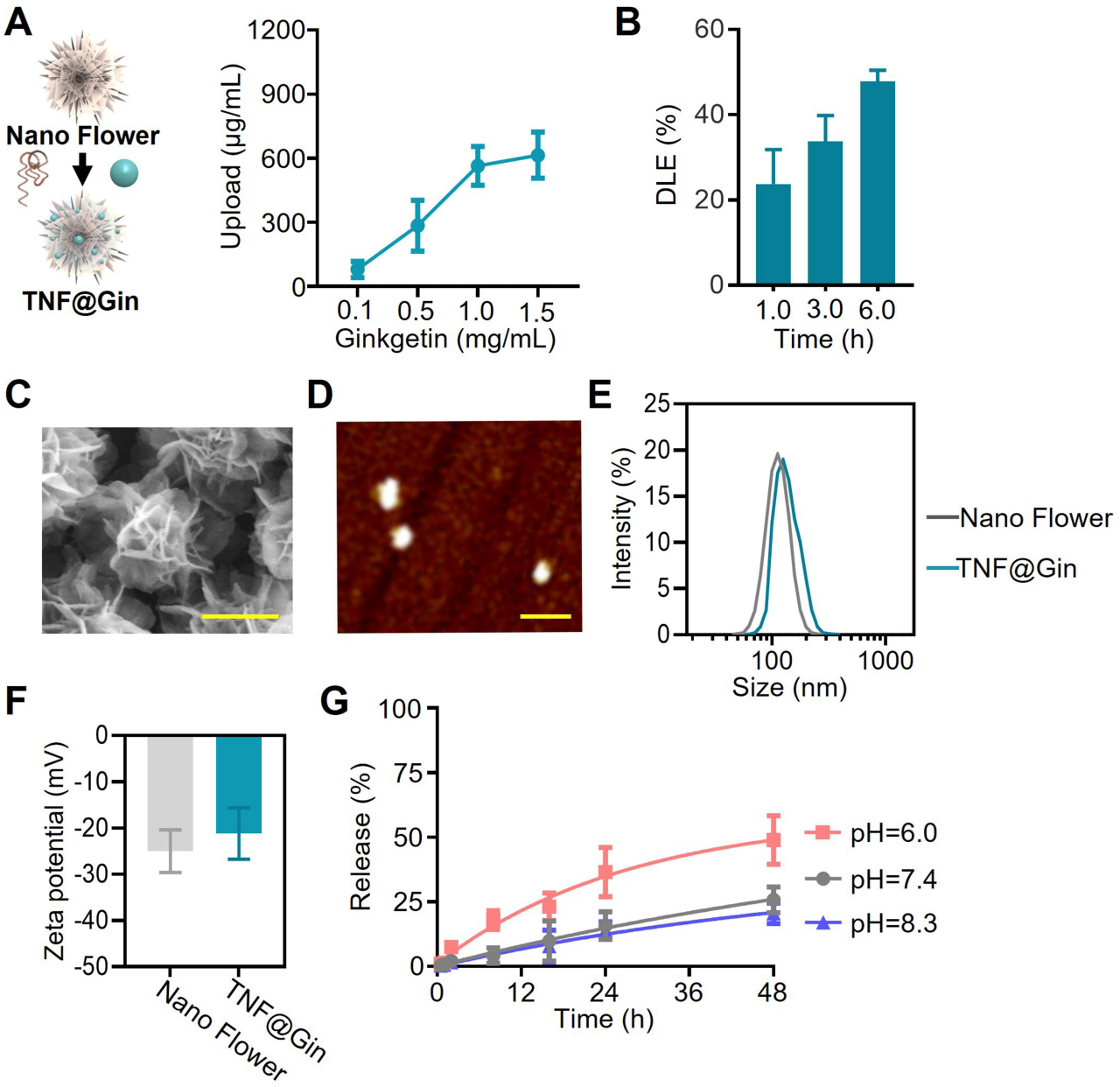

Figure 2 (**A**) Upload of Ginkgetin in TNF@Gin. The addition of Ginkgetin ranged from 0.1 to 1.5 mg/mL. (**B**) Drug loading efficiency (DLE) of TNF@Gin in Nano Flower measured by UV absorption. (**C**) Scanning electron microscopy (SEM) imaging of the TNF@Gin. Scale bar: 100 nm. (**D**) Atomic force microscope (AFM) imaging of the TNF@Gin under ScanAsyst-Air mode. Scale bar: 500 nm. (**E**) Hydrodynamic size analysis conducted by dynamic light scattering in PBS. (**F**) Zeta-potential of Nano Flower and TNF@Gin. (**G**) Time-dependent Ginkgetin release at different pH levels. TNF@Gin was separated in PBS with pH of 6.0, 7.4, or 8.3. The data are presented as mean ± SEM (n=3).

intensity nearly returning to the baseline level of the control group as quantitatively confirmed by statistical analysis (Figure 3B). Consistent with the ROS scavenging, the cell viability assay revealed that OxyHb induction caused notable cytotoxicity in BV2 cells. As expected, the TNF@Gin treatment provided the most significant protection against this damage, substantially improving cell survival compared to all other treatment groups (Figure 3C). Given the critical role of microglial polarization in the inflammatory response, we next investigated the effect of TNF@Gin on the M1/M2 phenotype balance. Immunofluorescence calculation was used to identify M1 macrophages (Iba1+CD16/32+) and M2 macrophages (Iba1+CD206+). The results showed that the treatment with TNF@Gin effectively reversed the trend in ICH, markedly decreasing the proportion of M1 cells and increasing the proportion of M2 cells (Figure 3D and E). Consequently, the M2/M1 ratio, a crucial indicator of the inflammatory state, was dramatically increased following

https://doi.org/10.2147/IJN.S590652

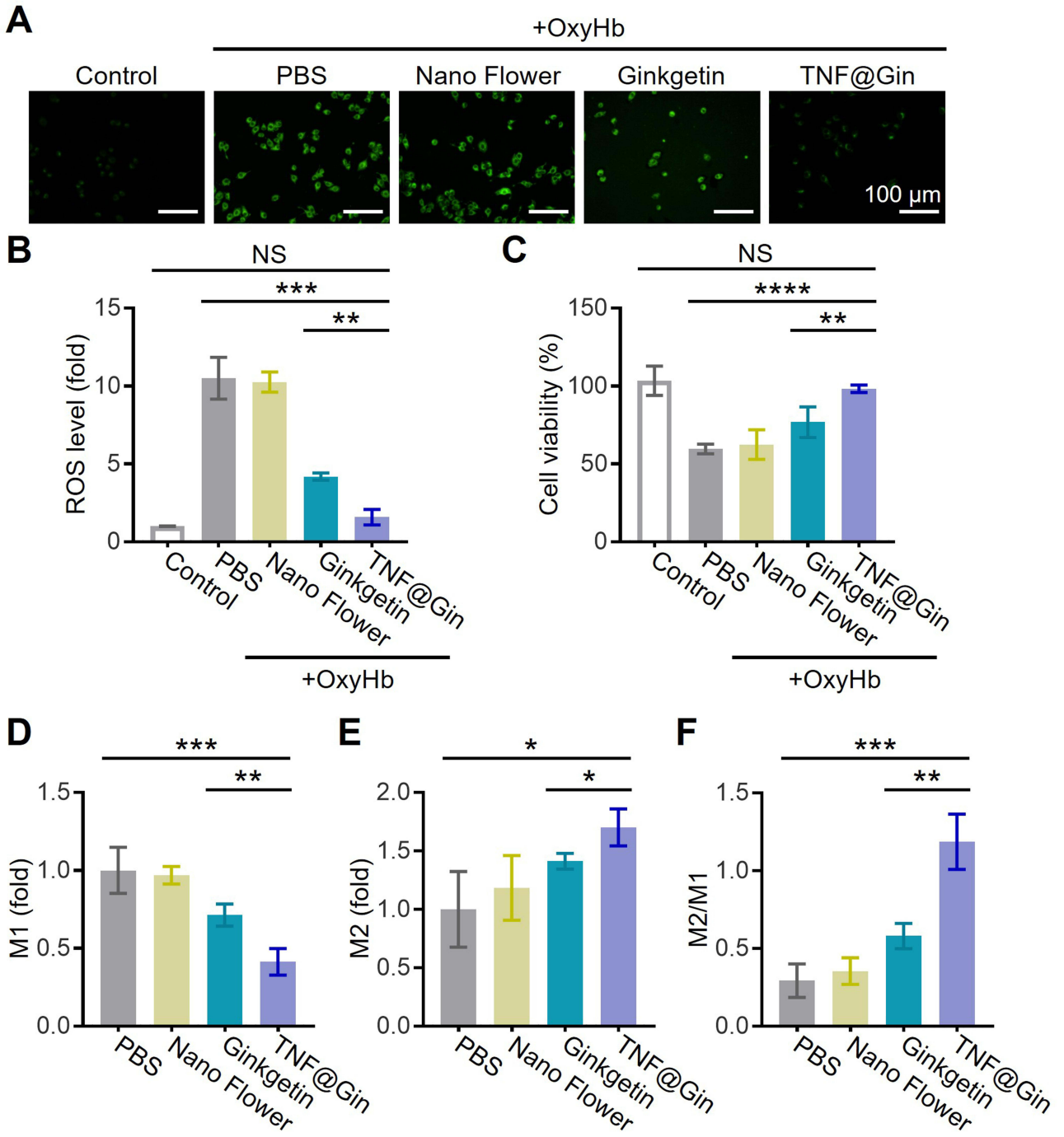

Figure 3 (**A**) Representative images of intracellular ROS levels measured using DCFH-DA in BV2 cells. Cells were treated with different components (PBS, Nano Flower, Ginkgetin, or TNF@Gin) after 24 h of induction of OxyHb. Scale bar: 100 μm. (**B**) Statistical analysis of the intracellular ROS. (**C**) Cell viability of BV2 cells treated with different components 24 h after OxyHb intervention. (**D** and **E**) Level of M1 (Iba1+CD16/32) cell and M2 (Iba1+CD206) cell in various groups. (**F**) Ratio of M2/M1 in various groups. The drug concentration was based on 1 μg mL^{-1} Ginkgetin. The concentration of the Nano Flower was calculated based on the nucleic acid concentration in TNF@Gin. The data are presented as mean ± SEM (n=3). Statistical significance was calculated by one-way analysis of variance (ANOVA) with the Tukey post hoc test, NS indicates not significant, * $p < 0.05$, ** $p < 0.01$, *** $p < 0.001$, **** $p < 0.0001$.

TNF@Gin intervention (Figure 3F). Taken together, these findings demonstrate that TNF@Gin effectively mitigates oxidative stress and cytotoxicity while concurrently reprogramming microglia from a pro-inflammatory M1 to an anti-inflammatory M2 phenotype. This dual-action mechanism highlights its considerable promise as a therapeutic strategy for managing the inflammatory pathologies associated with ICH.

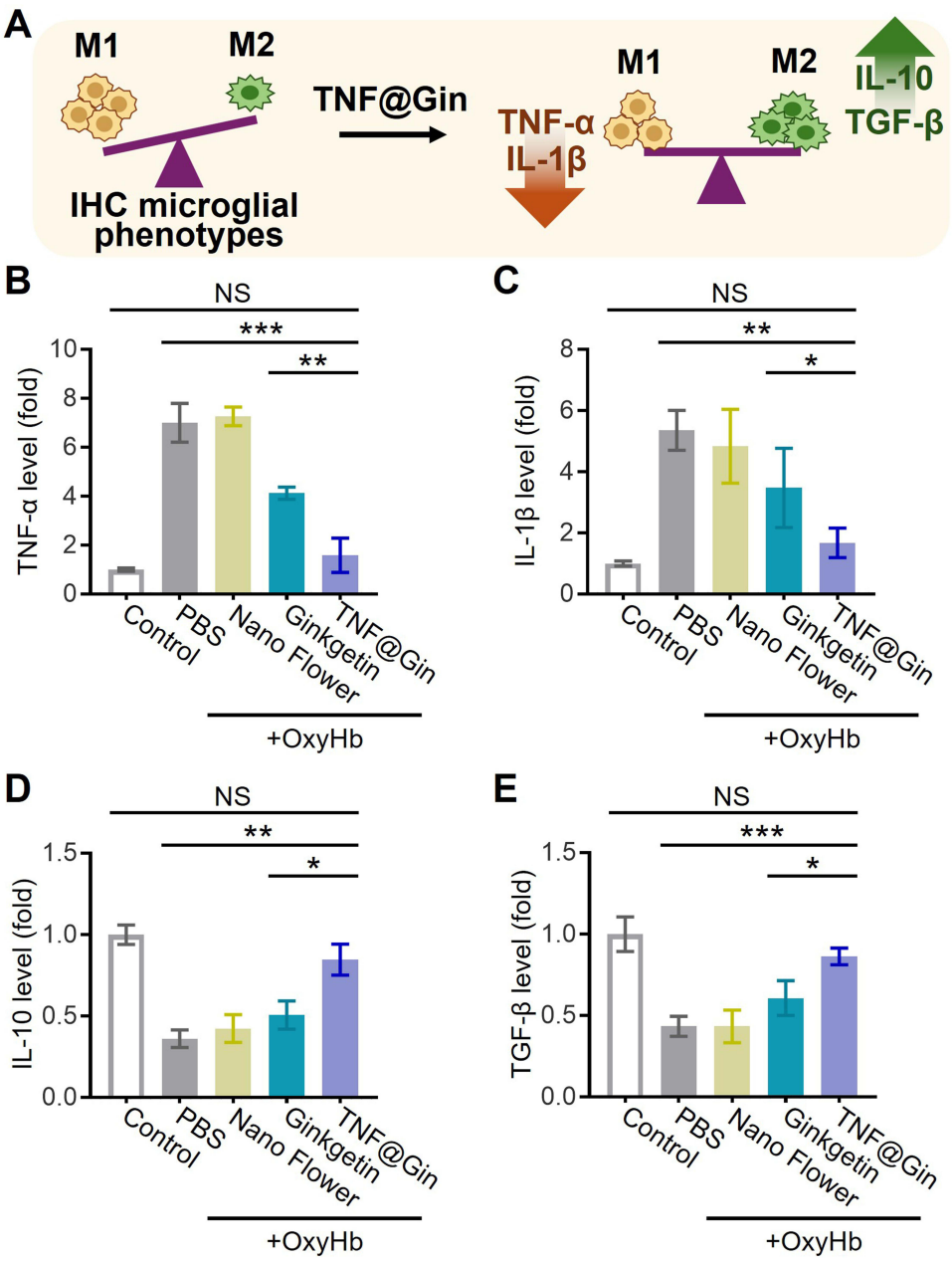

Figure 4 (**A**) Schematic illustration of the TNF@Gin regulating microglial phenotypes in BV2 cells. (**B** and **C**) Pro-inflammatory factors TNF-α and IL-1β in the BV2 cellular supernatant at 24 h detected via ELISA. (**D** and **E**) Anti-inflammatory factors IL-10 and TGF-β in the BV2 cellular supernatant at 24 h detected via ELISA. The drug concentration was based on 1 μg mL^{-1} Ginkgetin. The concentration of the Nano Flower was calculated based on the nucleic acid concentration in TNF@Gin. The data are presented as mean ± SEM (n=3). Statistical significance was calculated by one-way analysis of variance (ANOVA) with the Tukey post hoc test, NS indicates not significant, * $p < 0.05$, ** $p < 0.01$, *** $p < 0.001$.

To further elucidate the molecular mechanisms underlying the TNF@Gin-mediated regulation of microglial phenotypes, we quantified the key inflammatory cytokines in the supernatant of BV2 cells following OxyHb induction (Figure 4A). As shown in Figure 4B and C, OxyHb stimulation triggered a robust inflammatory response, leading to a significant increase in the secretion of both TNF-α and IL-1β compared to the control group. While treatment with the Nano Flower or free Ginkgetin resulted in a moderate reduction of these cytokines, the TNF@Gin group exhibited the most potent anti-inflammatory effect with the reductions being statistically significant. Next, we assessed the secretion of anti-inflammatory cytokines. As shown in Figure 4D and E, notably, TNF@Gin treatment effectively reversed the immunosuppressive effect, significantly elevating the concentrations of both IL-10 and TGF-β levels compared to Nano Flower and free drug treatment.

https://doi.org/10.2147/IJN.S590652

Evaluation of Nanomodulator-Mediated Attenuation of Ferroptosis

To investigate the potential of TNF@Gin to mitigate ferroptosis in neuronal cells, we employed OxyHb-induced HT22 cells as an ICH cell model. We first evaluated the intracellular ROS levels, as visualized by DCFH-DA fluorescence, treatment with TNF@Gin led to a significant reduction in intracellular ROS compared to the control group, demonstrating its potent antioxidant activity at the cellular level (Figure 5A). According to the cell viability assay, the nanomodulator TNF@Gin could also alleviate the cell toxicity induced by OxyHb (Figure S10). We then delved into the underlying molecular mechanisms by examining the key regulators of the antioxidant defense system. Quantitative PCR analysis

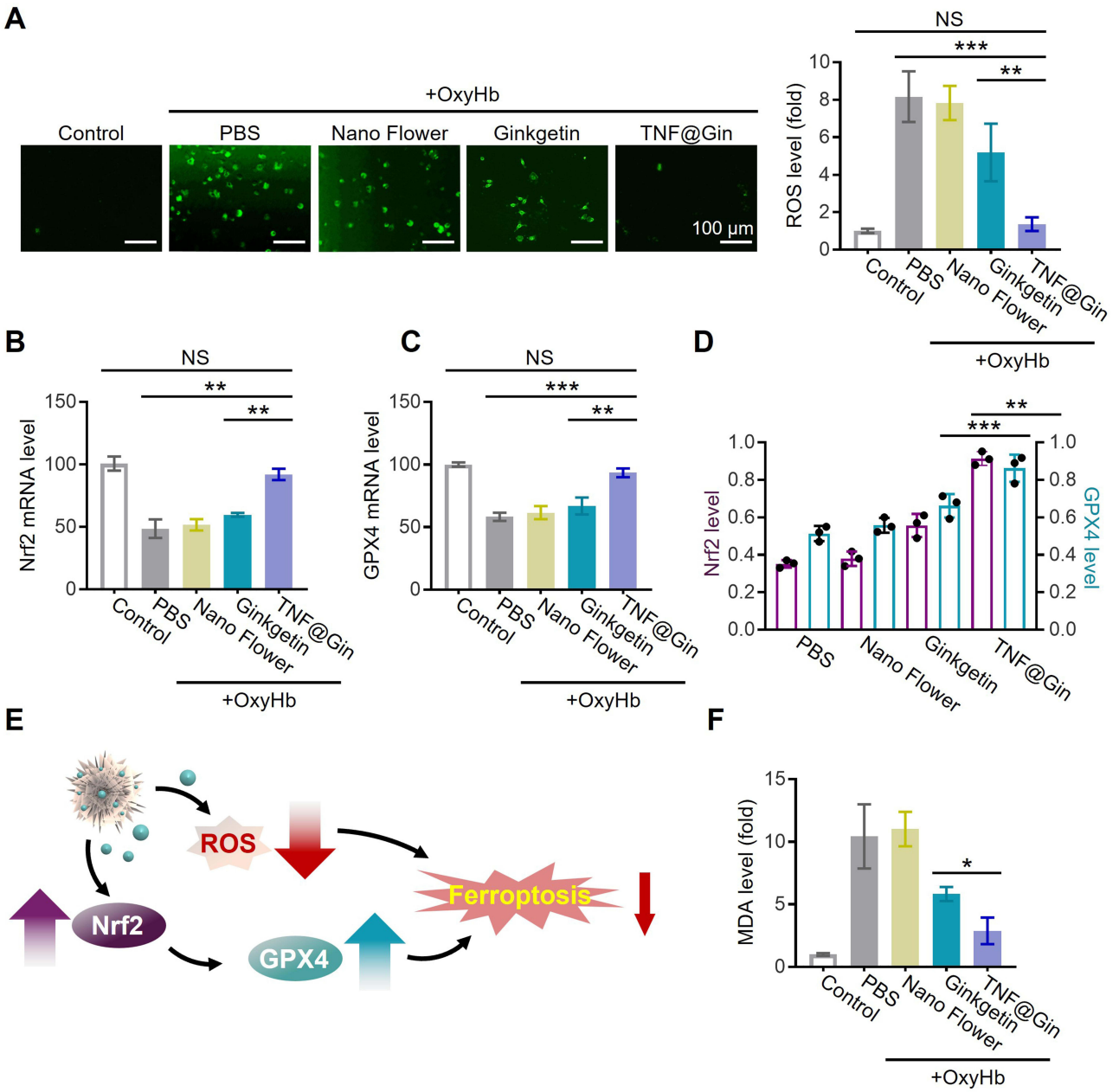

Figure 5 (**A**) Representative images and statistical analysis of intracellular ROS levels measured using DCFH-DA in HT22 cells. Scale bar = 100 μm. (**B** and **C**) The level of GPX4 and Nrf2 mRNA in HT22 cells assessed by quantitative-PCR. (**D**) Protein expression level of GPX4 and Nrf2 assessed by ELISA. (**E**) Schematic illustration of the mechanism in attenuating ferroptosis in HT22 cells. Red downward arrows indicate downregulation, while upward arrows indicate upregulation. (**F**) MDA levels in HT22 cells after various treatments. The drug concentration was based on 1 μg mL^{-1} Ginkgetin. The concentration of the Nano Flower was calculated based on the nucleic acid concentration in TNF@Gin. The data are presented as mean ± SEM (n=3). Statistical significance was calculated by one-way analysis of variance (ANOVA) with the Tukey post hoc test, NS indicates not significant, * $p < 0.05$, ** $p < 0.01$, *** $p < 0.001$.

https://doi.org/10.2147/IJN.S590652

revealed that TNF@Gin treatment significantly upregulated the mRNA expression of both glutathione peroxidase 4 (GPX4) and nuclear factor erythroid 2-related factor 2 (Nrf2) (Figure 5B and C). Consistent with these transcriptional changes, ELISA analysis confirmed a corresponding increase in the protein level of GPX4 and Nrf2 (Figure 5D). The upregulation of the key factor Nrf2, a master regulator of antioxidant responses, and its downstream effector GPX4, a central enzyme that inhibits lipid peroxidation, strongly suggests that TNF@Gin activates a protective cellular pathway against ferroptosis. This proposed mechanism is schematically illustrated in Figure 5E. Functionally, the activation of this anti-ferroptotic pathway was further validated by measuring malondialdehyde (MDA), a primary byproduct of lipid peroxidation and a well-established biomarker for ferroptosis. The results showed that TNF@Gin treatment significantly decreased the MDA levels in OxyHb-induced HT22 cells, indicating effective suppression of lipid peroxidation (Figure 5F). Collectively, these findings demonstrate that TNF@Gin effectively attenuates ferroptosis in HT22 cells through activating the Nrf2/GPX4 signaling axis.

Therapeutic Efficacy and Mechanistic Insights in ICH

To evaluate the therapeutic efficacy of TNF@Gin in vivo, we employed an ICH mouse model and conducted a comprehensive assessment encompassing behavioral tests, biochemical analysis, and histological examination over a 28-day treatment period. First, in the foot fault test, which measures fine motor coordination and placement deficits, mice treated with TNF@Gin (2 mg Ginkgetin/kg body weight through *i.v.)* showed a statistically significant reduction in the number of foot faults compared to the ICH group, indicating a marked improvement in motor function (Figure 6A). This functional recovery was further corroborated by the rotarod test. As shown in Figure 6B, TNF@Gin-treated mice demonstrated a significantly longer latency to fall, reflecting enhanced motor balance and coordination. As shown in Figure 6, significant differences for Ginkgetin and TNF@Gin were primarily observed at Day 28. This time-dependent trend can be attributed to a cumulative therapeutic effect. During the initial stages of treatment (Days 7–21), the therapeutic effects were accumulating. As the treatment progressed, sustained pharmacological action yielded a robust outcome by Day 28. To investigate the pathological and molecular basis for this improvement, we analyzed brain tissues from the treated mice. As shown in Figure 6C, treatment with the TNF@Gin significantly reduced MDA levels in the

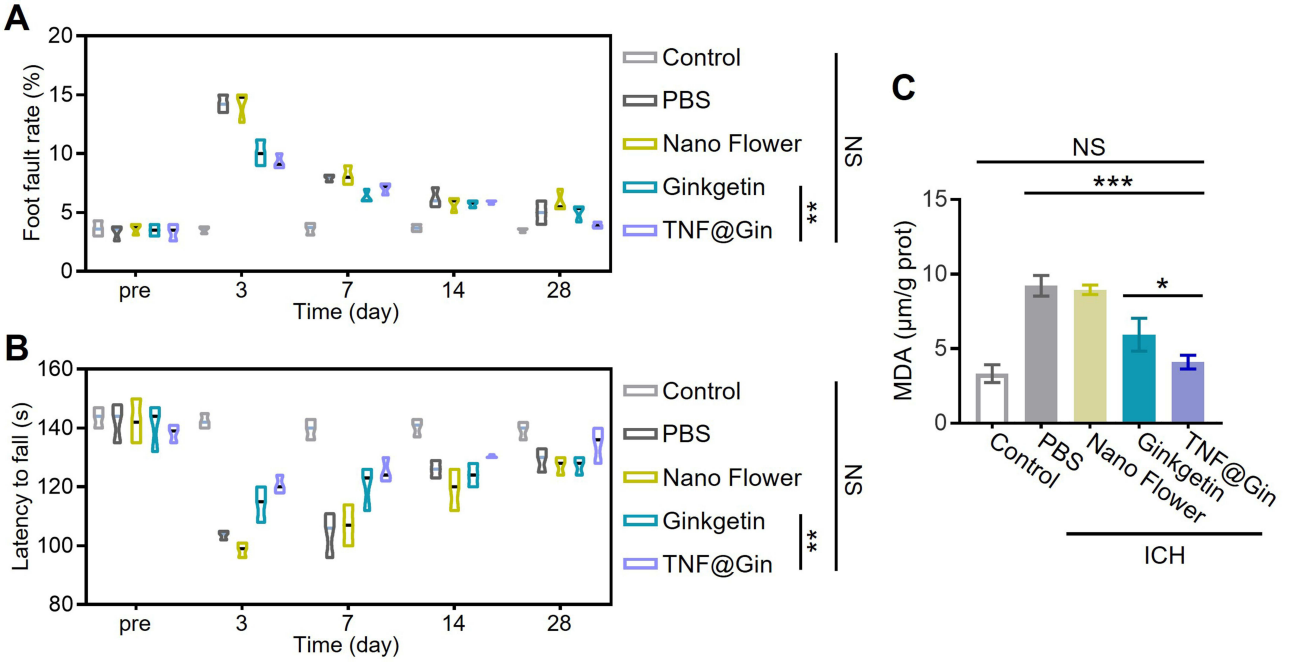

Figure 6 (**A**) Statistical analysis of the foot fault test during the 28 day of the treatment. (n=10). (**B**) Statistical analysis of the rotarod test during the 28 day of the treatment. (n=10). (**C**) MDA levels in brain extract from the ICH mouse. (n=3). Healthy mice were used as the control group. The drug concentration was based on 2 mg Ginkgetin/kg body weight. Statistical significance was calculated by one-way analysis of variance (ANOVA) with the Tukey post hoc test, NS indicates not significant, * $p < 0.05$, ** $p < 0.01$, *** $p < 0.001$.

https://doi.org/10.2147/IJN.S590652

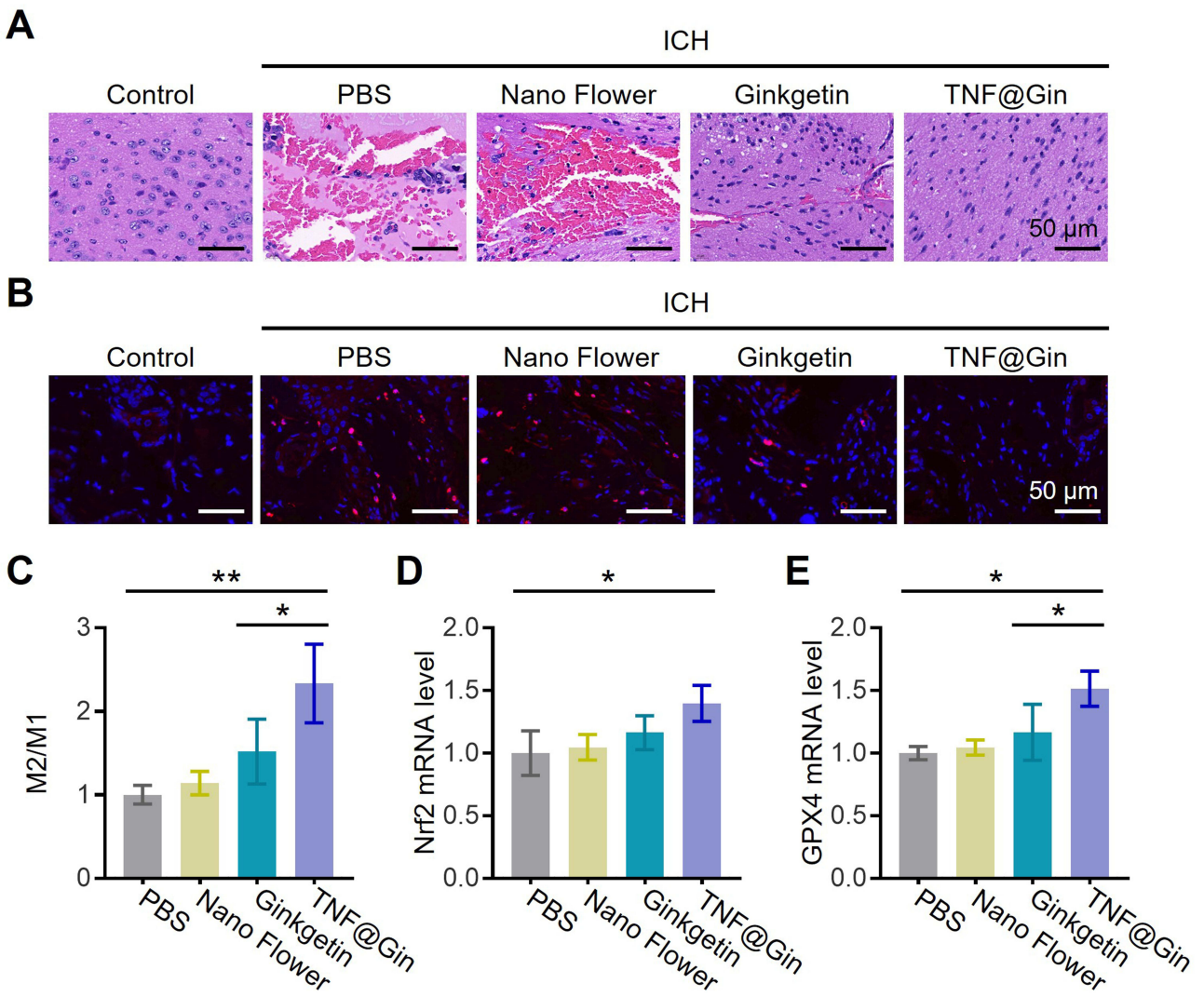

Figure 7 (**A**) Representative images of H&E staining of brain sections from ICH mice after different treatments. Scale bar = 50 μm. (**B**) Immunofluorescence images of ROS in brain sections. Scale bar = 50 μm. (**C**) Ratio of M2/M1 in brain tissues measured by ELISA. (**D** and **E**) The level of GPX4 and Nrf2 mRNA in brain tissues assessed by quantitative-PCR. The data are presented as mean ± SEM (n=5). Statistical significance was calculated by one-way analysis of variance (ANOVA) with the Tukey post hoc test, * $p < 0.05$, ** $p < 0.01$.

brain tissues of mice. Histological examination via H&E staining revealed that the ICH group suffered severe neuronal damage and tissue disorganization. In contrast, TNF@Gin treatment provided substantial neuroprotection, preserving the normal cellular architecture and reducing the extent of tissue injury (Figure 7A). Consistent with this, immunofluorescence staining for ROS showed that TNF@Gin administration led to a dramatic decrease in ROS accumulation in the brain sections, confirming its potent anti-oxidative stress effect in vivo (Figure 7B). We then quantified the M1/M2 polarization ratio in brain tissue (Figures S11 and S12). The level of M1 cells was notably elevated in the ICH group but was effectively reversed by TNF@Gin treatment, which lowered the ratio towards a more anti-inflammatory profile (Figure 7C). At the molecular level, quantitative-PCR analysis confirmed that TNF@Gin treatment significantly upregulated the mRNA expression of the key anti-ferroptotic proteins Nrf2 and GPX4 in brain tissues (Figure 7D and E). Collectively, these in vivo findings demonstrate that TNF@Gin treatment not only promotes significant long-term functional recovery but also exerts potent neuroprotective effects by mitigating oxidative stress, reducing lipid peroxidation, and modulating the inflammatory response in the brain following ICH. The superior efficacy of TNF@Gin over free Ginkgetin stems from the nano-delivery system's ability to overcome the inherent limitations of the free compound. While free Ginkgetin suffers from poor solubility and rapid clearance, TNF@Gin enhances solubility and protects the

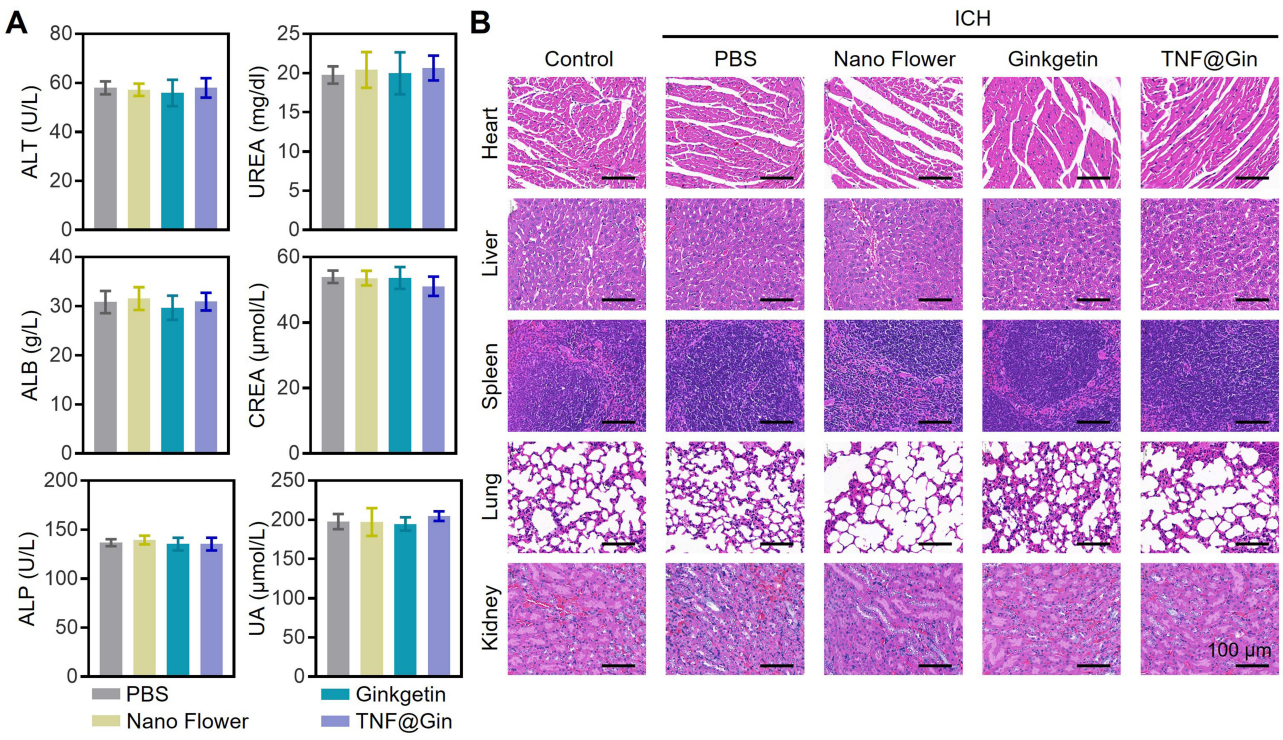

Figure 8 (**A**) Blood biochemical analysis after the treatment of PBS, Nano Flower, Ginkgetin, or TNF@Gin. (**B**) H&E staining of the liver, lung, kidney, heart, and spleen after the treatment. Scale bar: 100 μm. The data are presented as mean ± SEM (n=3).

flavonoid from oxidative inactivation, thereby maintaining pharmacological activity during circulation. Moreover, unlike the inefficient passive diffusion of free Ginkgetin, the nano-formulation facilitates cellular internalization via endocytosis, significantly increasing intracellular drug accumulation and therapeutic potency.

To assess the biocompatibility, blood samples were collected during the treatment, and blood index values were measured (alanine aminotransferase (ALT), alkaline phos-phatase (ALP), albumin (ALB), UREA, Creatinine (CREA), and uric acid (UA)). All the tested function markers remained within the normal ranges during the treatment (Figure 8A). Then, a histopathological examination was performed on major organs, including the heart, liver, spleen, lung, and kidney. H&E staining revealed that the cellular architecture and morphology of these organs in all treatment groups were well-preserved, with no signs of inflammation, cellular necrosis, edema, or other pathological lesions (Figure 8B). Moreover, no significant loss of body weight was observed, suggesting that the treatments did not induce acute adverse physiological effects or cause significant distress to the animals (Figure S13). The results prove that TNF@Gin is a promising nanoplatform for effective treatment of ICH. Distinct from existing literature that often reports transient therapeutic effects, our formulation demonstrated a sustained pharmacological action resulting in significant long-term benefits. This time-dependent cumulative effect, as evidenced by the histological and functional recovery data, suggests that the TNF@Gin nanomodulator offers a pharmacokinetic advantage over formulations reported in earlier works, providing a more durable protection against secondary brain injury.

Conclusion

In this study, we successfully developed a Ginkgetin-loaded nanoflower, TNF@Gin, and systematically evaluated its therapeutic potential and underlying mechanisms in treating ICH. The nanomodulator exhibited favorable physicochemical properties, including a uniform morphology, high loading capacity, and excellent stability. In both in vitro and in vivo ICH models, TNF@Gin provided potent neuroprotection by targeting the core pathological cascades of secondary brain injury. Mechanistically, TNF@Gin effectively scavenged reactive oxygen species, reprogrammed microglia from a pro-inflammatory M1 phenotype to an anti-inflammatory M2 phenotype, and mitigated neuronal ferroptosis by activating the

https://doi.org/10.2147/IJN.S590652

Nrf2/GPX4 signaling axis. These multifaceted actions culminated in significant long-term functional recovery in treated ICH mice. Critically, the nanomodulator demonstrated excellent biocompatibility with no observable systemic toxicity. Taken together, our findings present TNF@Gin as a safe and highly effective nanotherapeutic strategy that holds immense promise for the clinical management of ICH.

Abbreviations

ICH, intracerebral hemorrhage; RCA, rolling circle amplification; BBB, blood-brain barrier; ROS, reactive oxygen species; DTT, dithiothreitol; FBS, fetal bovine serum; CCK-8: cell counting kit 8; ATCC, American type culture collection; ATP, adenosine triphosphate; DLE, drug loading efficiency; AFM, atomic force microscopy; TNF-α, tumor necrosis factor-α; IL-1β, interleukin-1β; IL-10, interleukin-10; TGF-β, transforming growth factor-β; ELISA, enzyme-linked immunosorbent assay; H&E, hematoxylin and eosin; TEM, transmission electron microscope; GPX4, glutathione peroxidase 4; Nrf2, nuclear factor erythroid 2-related factor 2; MDA, malondialdehyde; ALT, alanine aminotransferase; ALP, alkaline phos-phatase; ALB, albumin; CREA, creatinine; UA, uric acid.

Acknowledgments

This work was supported by the Hainan Provincial Natural Science Foundation of China (824QN261) and Academic Enhancement Support Program of Hainan Medical University (XSTS2025107). The authors are grateful to the support of instruments and facilities provided by Public Research Center of Hainan Medical University.

Author Contributions

All authors made a significant contribution to the work reported, whether that is in the conception, study design, execution, acquisition of data, analysis and interpretation, or in all these areas; took part in drafting, revising or critically reviewing the article; gave final approval of the version to be published; have agreed on the journal to which the article has been submitted; and agree to be accountable for all aspects of the work.

Disclosure

The authors report no conflicts of interest in this work.

References

1. Puy L, Parry-Jones AR, Sandset EC, Dowlatshahi D, Ziai W, Cordonnier C. Intracerebral haemorrhage. *Nat Rev Dis Primers*. 2023;9(1):14. doi:10.1038/s41572-023-00424-7
2. Seiffge DJ, Fandler-Höfler S, Du Y, et al. Intracerebral haemorrhage — mechanisms, diagnosis and prospects for treatment and prevention. *Nat Rev Neurol*. 2024;20(12):708–723. doi:10.1038/s41582-024-01035-w
3. Xue M, Yong VW. Neuroinflammation in intracerebral haemorrhage: immunotherapies with potential for translation. *Lancet Neurol*. 2020;19(12):1023–1032. doi:10.1016/S1474-4422(20)30364-1
4. Morotti A, Boulouis G, Dowlatshahi D, et al. Intracerebral haemorrhage expansion: definitions, predictors, and prevention. *Lancet Neurol*. 2023;22(2):159–171. doi:10.1016/S1474-4422(22)00338-6
5. Yang Q, Enríquez Á, Devathasan D, et al. Application of magnetically actuated self-clearing catheter for rapid in situ blood clot clearance in hemorrhagic stroke treatment. *Nat Commun*. 2022;13(1):520. doi:10.1038/s41467-022-28101-5
6. Li X-N, Lin L, Li X-W, et al. BSA-stabilized selenium nanoparticles ameliorate intracerebral hemorrhage's-like pathology by inhibiting ferroptosis-mediated neurotoxicology via Nrf2/GPX4 axis activation. *Redox Biol*. 2024;75:103268. doi:10.1016/j.redox.2024.103268
7. Xiao Z, Shen D, Lan T, et al. Reduction of lactoferrin aggravates neuronal ferroptosis after intracerebral hemorrhagic stroke in hyperglycemic mice. *Redox Biol*. 2022;50:102256. doi:10.1016/j.redox.2022.102256
8. Yang Y, Gao L, Xi J, et al. Mesenchymal stem cell-derived extracellular vesicles mitigate neuronal damage from intracerebral hemorrhage by modulating ferroptosis. *Stem Cell Res Ther*. 2024;15(1):255. doi:10.1186/s13287-024-03879-x
9. Jiang Z, Yang H, Ni W, et al. Attenuation of neuronal ferroptosis in intracerebral hemorrhage by inhibiting HDAC1/2: microglial heterogenization via the Nrf2/HO1 pathway. *CNS Neurosci Therap*. 2024;30(3):e14646. doi:10.1111/cns.14646
10. Li Q, Han X, Lan X, et al. Inhibition of neuronal ferroptosis protects hemorrhagic brain. *JCI Insight*. 2017;2(7):e90777. doi:10.1172/jci.insight.90777
11. Zhou Z-X, Cui Q, Zhang Y-M, et al. Withaferin A inhibits ferroptosis and protects against intracerebral hemorrhage. *Neural Regen Res*. 2023;18(6):1308–1315. doi:10.4103/1673-5374.355822
12. Zeng Y, Liu J, Kong Z, et al. Catechin-based polyphenol nanoparticles ameliorated ferroptosis to alleviate brain injury after intracerebral hemorrhage. *ACS Appl Mater Interfaces*. 2025;17(5):7424–7437. doi:10.1021/acsami.4c19513

13. Loan JJM, Kirby C, Emelianova K, et al. Secondary injury and inflammation after intracerebral haemorrhage: a systematic review and meta-analysis of molecular markers in patient brain tissue. *J Neurol Neurosurg Psychiatry*. 2022;93(2):126. doi:10.1136/jnnp-2021-327098
14. Li Y, Zhou H, He X, et al. Impaired microglial glycolysis promotes inflammatory responses after intracerebral haemorrhage via HK2-dependent mitochondrial dysfunction. *J Adv Res*. 2025;73:575–591. doi:10.1016/j.jare.2024.08.016
15. Lan X, Han X, Li Q, Yang Q-W, Wang J. Modulators of microglial activation and polarization after intracerebral haemorrhage. *Nat Rev Neurol*. 2017;13(7):420–433. doi:10.1038/nrneurol.2017.69
16. Yu W, Che C, Yang Y, et al. Bioactive self-assembled nanomodulator enhances hematoma resolution and inhibits neuroinflammation in the treatment of intracerebral hemorrhage. *Adv Sci*. 2025;12(1):2408647. doi:10.1002/advs.202408647
17. Shih-Ho L, Abel Po-Hao H, Shan-hui H. Injectable, micellar chitosan self-healing hydrogel for asynchronous dual-drug delivery to treat stroke rats. *Adv Funct Mater*. 2023;33(45):2303853. doi:10.1002/adfm.202303853
18. Wu G, Liu Z, Mu C, et al. Enhanced proliferation of visualizable mesenchymal stem cell–platelet hybrid cell for versatile intracerebral hemorrhage treatment. *ACS Nano*. 2023;17(8):7352–7365. doi:10.1021/acsnano.2c11329
19. Zhang S, Li R, Song M, Han J, Fan X. Exploration of M2 macrophage membrane as a biotherapeutic agent and strong synergistic therapeutic effects in ischemic stroke. *J Control Release*. 2025;378:476–489. doi:10.1016/j.jconrel.2024.11.033
20. Stater EP, Sonay AY, Hart C, Grimm J. The ancillary effects of nanoparticles and their implications for nanomedicine. *Nat Nanotechnol*. 2021;16(11):1180–1194. doi:10.1038/s41565-021-01017-9
21. de Almeida M S, Susnik E, Drasler B, Taladriz-Blanco P, Petri-Fink A, Rothen-Rutishauser B. Understanding nanoparticle endocytosis to improve targeting strategies in nanomedicine. *Chem Soc Rev*. 2021;50(9):5397–5434. doi:10.1039/D0CS01127D
22. Serov N, Vinogradov V. Artificial intelligence to bring nanomedicine to life. *Adv Drug Deliv Rev*. 2022;184:114194.10.1016/j.addr.2022.114194
23. Hu Q, Li H, Wang L, Gu H, Fan C. DNA nanotechnology-enabled drug delivery systems. *Chem Rev*. 2019;119(10):6459–6506. doi:10.1021/acs.chemrev.7b00663
24. Ali MM, Li F, Zhang Z, et al. Rolling circle amplification: a versatile tool for chemical biology, materials science and medicine. *Chem Soc Rev*. 2014;43(10):3324–3341. doi:10.1039/C3CS60439J
25. Mao D, Li W, Liu X, et al. Rolling-circle-amplification-based DNA-enzyme nanostructure for immobilization and functionalization of enzymes. *Chem*. 2025;11(2). doi:10.1016/j.chempr.2024.10.002
26. Andersen ES, Dong M, Nielsen MM, et al. Self-assembly of a nanoscale DNA box with a controllable lid. *Nature*. 2009;459(7243):73–76. doi:10.1038/nature07971
27. Lee JH, Ku SH, Kim MJ, et al. Rolling circle transcription-based polymeric siRNA nanoparticles for tumor-targeted delivery. *J Control Release*. 2017;263:29–38. doi:10.1016/j.jconrel.2017.03.390
28. Tian R, Wang Y, Wang H, et al. Self-assembled multifunctional DNA nanoparticles for targeted rheumatoid arthritis therapy. *CCS Chemistry*. 2025;7(6):1745–1759. doi:10.31635/ccschem.025.202505735
29. Yao C, Zhang R, Tang J, Yang D. Rolling circle amplification (RCA)-based DNA hydrogel. *Nat Protocols*. 2021;16(12):5460–5483. doi:10.1038/s41596-021-00621-2
30. Yao C, Tang H, Wu W, et al. Double rolling circle amplification generates physically cross-linked DNA network for stem cell fishing. *J Am Chem Soc*. 2020;142(7):3422–3429. doi:10.1021/jacs.9b11001
31. Lou J-S, Zhao L-P, Huang Z-H, et al. Ginkgetin derived from Ginkgo biloba leaves enhances the therapeutic effect of cisplatin via ferroptosis-mediated disruption of the Nrf2/HO-1 axis in EGFR wild-type non-small-cell lung cancer. *Phytomedicine*. 2021;80:153370. doi:10.1016/j.phymed.2020.153370
32. Chun Hin L, Hei Tung S, Jiaxin L, et al. Splenectomy improves outcome of intracerebral hemorrhage. *FASEB J*. 2025:39e7051. doi:10.1096/fj.202500191R
33. Adnan M, Rasul A, Hussain G, et al. Ginkgetin: a natural biflavone with versatile pharmacological activities. *Food Chem Toxicol*. 2020;145:111642. doi:10.1016/j.fct.2020.111642
34. Tiantian W, Jianbing L, Manman L, et al. A Nanobody-Conjugated DNA Nanoplatform for Targeted Platinum-Drug Delivery. *Angewandte Chemie Int Ed*. 2019;58:14224–14228. doi:10.1002/anie.201909345
35. Tiantian W, Hong W, Run T, et al. A DNA origami-based bactericide for efficient healing of infected wounds. *Angewandte Chemie Int Ed*. 2023;62:e202311698. doi:10.1002/ange.202311698